SOLAR CELLS

Organometallic-functionalized interfaces for highly efficient inverted perovskite solar cells

Zhen Li[1]†, Bo Li[1]†, Xin Wu[1]†, Stephanie A. Sheppard[2], Shoufeng Zhang[1], Danpeng Gao[1], Nicholas J. Long[2]*, Zonglong Zhu[1,3]*

Further enhancing the performance and stability of inverted perovskite solar cells (PSCs) is crucial for their commercialization. We report that the functionalization of multication and halide perovskite interfaces with an organometallic compound, ferrocenyl-bis-thiophene-2-carboxylate ($FcTc_2$), simultaneously enhanced the efficiency and stability of inverted PSCs. The resultant devices achieved a power conversion efficiency of 25.0% and maintained >98% of their initial efficiency after continuously operating at the maximum power point for 1500 hours under simulated AM1.5 illumination. Moreover, the $FcTc_2$-functionalized devices passed the international standards for mature photovoltaics (IEC61215:2016) and have exhibited high stability under the damp heat test (85°C and 85% relative humidity).

Power conversion efficiencies (PCEs) as high as 25.7% have been realized for single-junction conventional n-i-p perovskite solar cells (PSCs), approaching the PCEs of state-of-the-art crystalline-silicon solar cells (*1*–*3*). Inverted (p-i-n structure) devices, with a deposition sequence of hole-transport (p), intrinsic (i), and electron-transport (n) layers, have exhibited greater stabilities and lifetimes because of their undoped hole-transporting layers (HTLs) and the formation of highly crystalline perovskite films (*4*–*10*). Recently, strategies for managing defects and ion migration in inverted PSCs have further contributed to device stability. For example, Chen *et al*. have used solid-state carbohydrazide to modulate the crystallization of perovskites and fabricate a minimodule that maintained 85% of its initial PCE under 1-sun illumination (where 1 sun is defined as the standard illumination at AM1.5, or 1 kW m^{-2}) for 1000 hours (*11*), and Bai *et al*. have applied ionic liquids within perovskite films by suppressing ion migration and have fabricated PSCs that exhibited only ~5% degradation of device performance under continuous simulated AM1.5 irradiation for >1800 hours (*12*). However, the currently reported operational lifetime of inverted PSCs under international standards still lags far behind the 25-year lifetime guarantee for commercialized silicon solar cells (*2*, *13*). Moreover, although synergistic tailoring of grains, defects, and interfaces can boost efficiencies to 23.3%, there is still a lack of strategy that could result in efficiencies of up to 25% to rival n-i-p PSCs and silicon solar cells (*14*–*16*).

[1]Department of Chemistry, City University of Hong Kong, Kowloon 999077, Hong Kong. [2]Department of Chemistry, Imperial College London, White City Campus, London, UK. [3]Hong Kong Institute of Clean Energy, City University of Hong Kong, Kowloon 999077, Hong Kong. [4]Hong Kong Institute of Clean Energy, City University of Hong Kong, Kowloon 999077, Hong Kong.
*Corresponding author. Email: zonglzhu@cityu.edu.hk (Z.Z.); n.long@imperial.ac.uk (N.J.L.)
†These authors contributed equally to this work.

Here, we report highly efficient and stable inverted PSCs through interface functionalization with an organometallic compound, ferrocenyl-bis-thiophene-2-carboxylate ($FcTc_2$), that not only provided strong chemical Pb-O binding to reduce surface trap states but also accelerated interfacial electron transfer through the electron-rich and electron-delocalizable ferrocene units. The improved interface binding and carrier transport properties of $FcTc_2$ contribute to superior device stability. The resulting devices achieved a PCE of 25.0% (with certified 24.3%) and maintained >98% of their initial efficiency in long-term operational stability tests with continuous 1-sun illumination for >1500 hours. Moreover, the $FcTc_2$-treated devices exhibited excellent stability under damp heat tests [85°C and 85% relative humidity (RH)], which have passed the international standards for silicon solar cells.

Interfaces were functionalized with $FcTc_2$ by using the inherent carboxylate and thiophene groups around the central ferrocene motif (see Fig. 1A for chemical structure). The ultraviolet-visible (UV-vis) absorption spectra of $FcTc_2$ in solution and as a thin film are shown in figs. S1 and S2, respectively. The device configuration is depicted in Fig. 1A, in which poly(triaryl amine) (PTAA) was the HTL and C_{60} was the electron transfer layer (ETL). Figure S3 shows the cross-sectional scanning electron microscopy (SEM) image of a typical device with a perovskite composition of $Cs_{0.05}(FA_{0.98}MA_{0.02})_{0.95}Pb(I_{0.98}Br_{0.02})_3$ (where MA and FA denote methylammonium and formamidinium, respectively) and $FcTc_2$ surface treatment. Time-of-flight secondary ion mass spectrometry (TOF-SIMS) in Fig. 1B demonstrates that most of the $FcTc_2$ was located on the surface of the perovskite film. We used x-ray diffraction (XRD), top-view SEM, and UV-vis absorption spectroscopy measurements to study the crystallinity, morphology, and optical absorption of perovskite films with and without $FcTc_2$ treatment (figs. S4 to S6). All of the samples showed no obvious changes, which indicates that $FcTc_2$ does not affect the crystallization and light-harvesting properties of perovskite films.

The interaction of $FcTc_2$ with the perovskite was studied by comparing the x-ray photoelectron spectroscopy (XPS) measurements on the pristine and $FcTc_2$-treated perovskite films (Fig. 1, C to E). The binding energies corresponding to the Pb 4f, I 3d, and N 1s core levels of the $FcTc_2$-treated perovskite films all shifted marginally to higher values compared with the control sample, suggesting enhanced binding of both anions and cations on the perovskite surface, which could be caused by strong binding between surface ions and $FcTc_2$ (*17*).

Density functional theory (DFT) simulation analyses were performed to study the interaction between the perovskite surface and $FcTc_2$ molecules. We chose the (001) PbI_2-terminated perovskite surface as a model because it has been proven to be stable and to have the lowest energy configuration. Starting from the ordered interface, we observed enhanced bonding of O from $FcTc_2$ with Pb from the perovskite surface within a few picoseconds (Fig. 1, F and G). With the interfacial rearrangement, the molecular dynamics reach a stable equilibrium state in which the bond length of Pb-O was simulated to be 2.65 Å (Fig. 1H). The electrostatic potential (ESP) analysis (fig. S7) indicated a high electronegativity (−29.79 kcal mol^{-1}) of O in $FcTc_2$, driving the formation of stable Pb-O bonds and substantially enhancing the electrostatic attraction between the perovskite and $FcTc_2$ interface. XPS analysis combined with DFT simulation proves that there is a strong interaction between perovskite and $FcTc_2$, which is beneficial for both passivation of surface defects and stabilization of surface components in perovskite (*7*, *18*).

To study the effect of $FcTc_2$ on the electrical properties of perovskite films, we conducted kelvin probe force microscopy (KPFM) measurements to examine the surface potential of the films (Fig. 2, A and B). The perovskite film functionalized by $FcTc_2$ exhibited a decreased contact potential (~50 mV) relative to that of the control sample, which suggests direct interaction and surface charge transfer between $FcTc_2$ and perovskite (*18*). Moreover, $FcTc_2$-functionalized perovskite displayed a smaller potential distribution and surface potential difference (~150 mV) compared with that of the control sample (~250 mV). A uniform distribution of surface contact potential was beneficial for effective charge carrier extraction to prevent nonradiative recombination (*19*, *20*). The carrier kinetics characterization (figs. S8 and S9) on the perovskite-ETL interface further verifies the accelerated electron extraction with $FcTc_2$ modification, which can be attributed to the ferrocene and thiophene units (*21*, *22*).

Time-resolved photoluminescence (TRPL) spectra were measured to evaluate the nonradiative

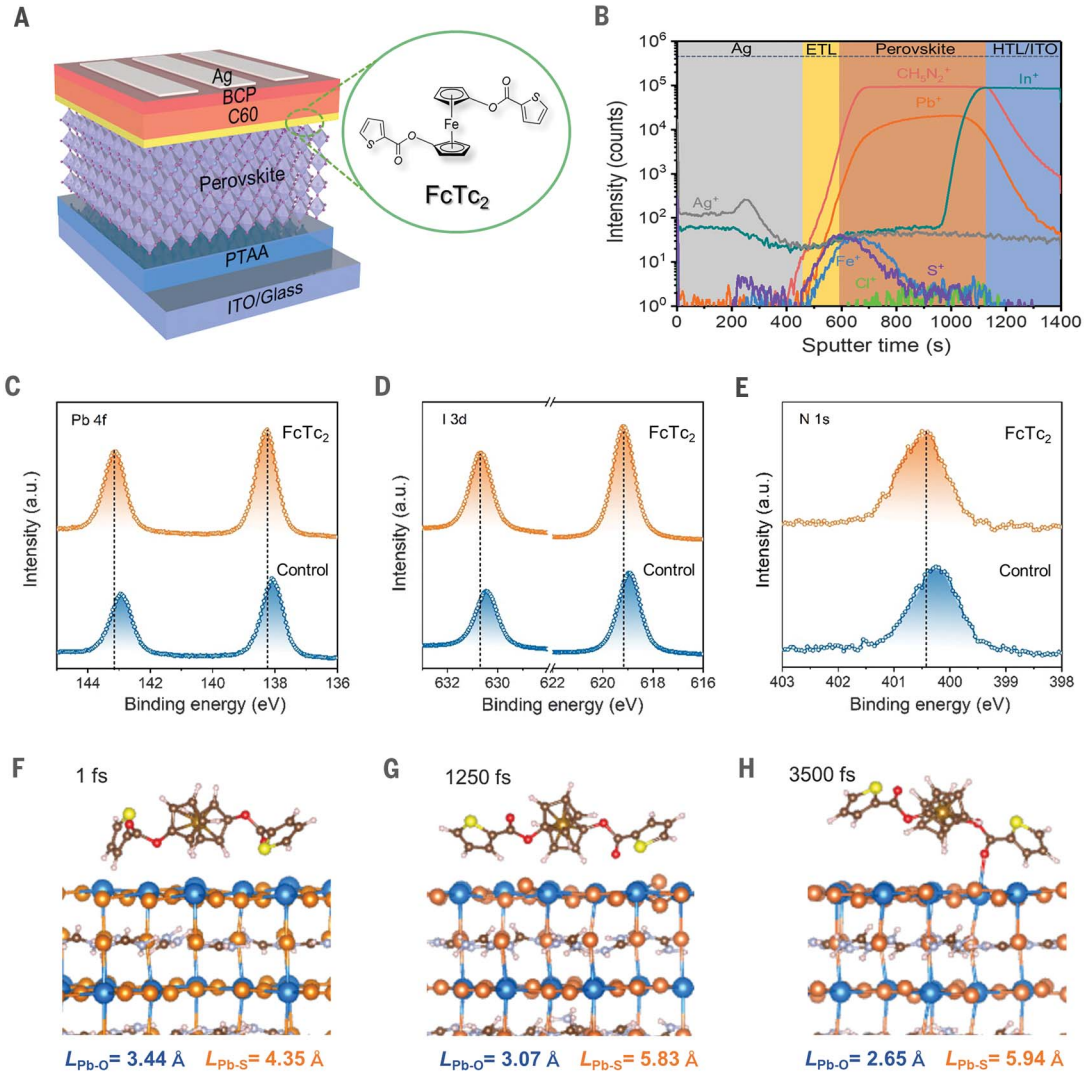

Fig. 1. Metal halide perovskite surface functionalized by $FcTc_2$. (**A**) Schematic illustration of inverted PSC based on $FcTc_2$ as the interface functionalization material. BCP, bathocuproine; ITO, indium tin oxide. (**B**) TOF-SIMS characterization of the PSC. (**C** to **E**) XPS characterization of Pb element (C), I element (D), and N element (E) on the perovskite film with and without $FcTc_2$. a.u., arbitrary units. (**F** to **H**) Molecular dynamics simulations of the interaction between perovskite and $FcTc_2$. *L*, bond length.

recombination of perovskite films (Fig. 2C). The carrier lifetime nearly doubled from 1166.74 to 2159.22 ns after incorporating $FcTc_2$ (the fitted carrier lifetime is summarized in table S1), which is consistent with enhanced steady-state photoluminescence intensity (fig. S10), indicating reduced numbers of nonradiative recombination centers from the surface defects. Additionally, the space charge–limited current (SCLC) measurements (fig. S12) further confirm the decreased defect density through $FcTc_2$ modification.

In triple-cation mixed-halide perovskite, the chemically reactive components, such as MA^+ and I^- at the perovskite surface, can easily volatilize and migrate through photo- and thermal effects. The surface trap states generate decreased photovoltaic performance degradation (*23*, *24*). To estimate the effect of $FcTc_2$ on perovskite stability, the MA^+ cations of the control and $FcTc_2$-functionalized perovskite films were probed by peak force infrared (PFIR) microscopy under illumination and heat conditions (*20*). The Fourier transform infrared (FTIR) spectroscopy spectra of the perovskite films confirmed that the signal of the MA ions in perovskite is distinct and readily resolved (fig. S13). PFIR mapping showed that the intensity and distribution of MA^+ cations in the $FcTc_2$-treated sample were well maintained after aging for 1000 hours (Fig. 2, D and F), whereas the control sample exhibited substantial reduction of intensity and broadening of distribution of the MA signal (Fig. 2, E and G). These results indicate that $FcTc_2$ can prevent surface ions from migration to produce a more uniform and stable surface component distribution (Fig. 2H) (*25*). By contrast, ion migration and volatilization were more prone to occur in the control films, resulting in increased surface defects and affecting the operational stability of perovskite devices (fig. S14). Measuring the perovskite films after >1000 hours separately under continuous 1-sun illumination or heating at 85°C also confirmed the stabilization effects of $FcTc_2$ on perovskite (figs. S15 and S16).

Figure 3A shows the current density–voltage (*J-V*) curves for control and $FcTc_2$-functionalized devices under AM1.5G simulated solar illumination, in which the concentration of $FcTc_2$ was optimized to be 1.0 mg ml^{-1} to obtain the best performance (figs. S17 and S18 and table S2). The control device exhibited a maximum PCE of 23.0%, with an open-circuit voltage (V_{OC}) of 1.13 V, a short-circuit current density (J_{SC}) of 25.25 mA cm^{-2}, and a fill factor (FF) of 80.45%. Compared with the control device, the $FcTc_2$-functionalized device exhibited an enhanced PCE of 25.0%, with an increased V_{OC} of 1.184 V, a J_{SC} of 25.68 mA cm^{-2}, and an FF of 82.32% with a low hysteresis (fig. S19). Corresponding external quantum efficiency (EQE) spectra (Fig. 3B) yielded integrated J_{SC} values with a small variation from the values obtained from *J-V* measurements. $FcTc_2$-treated

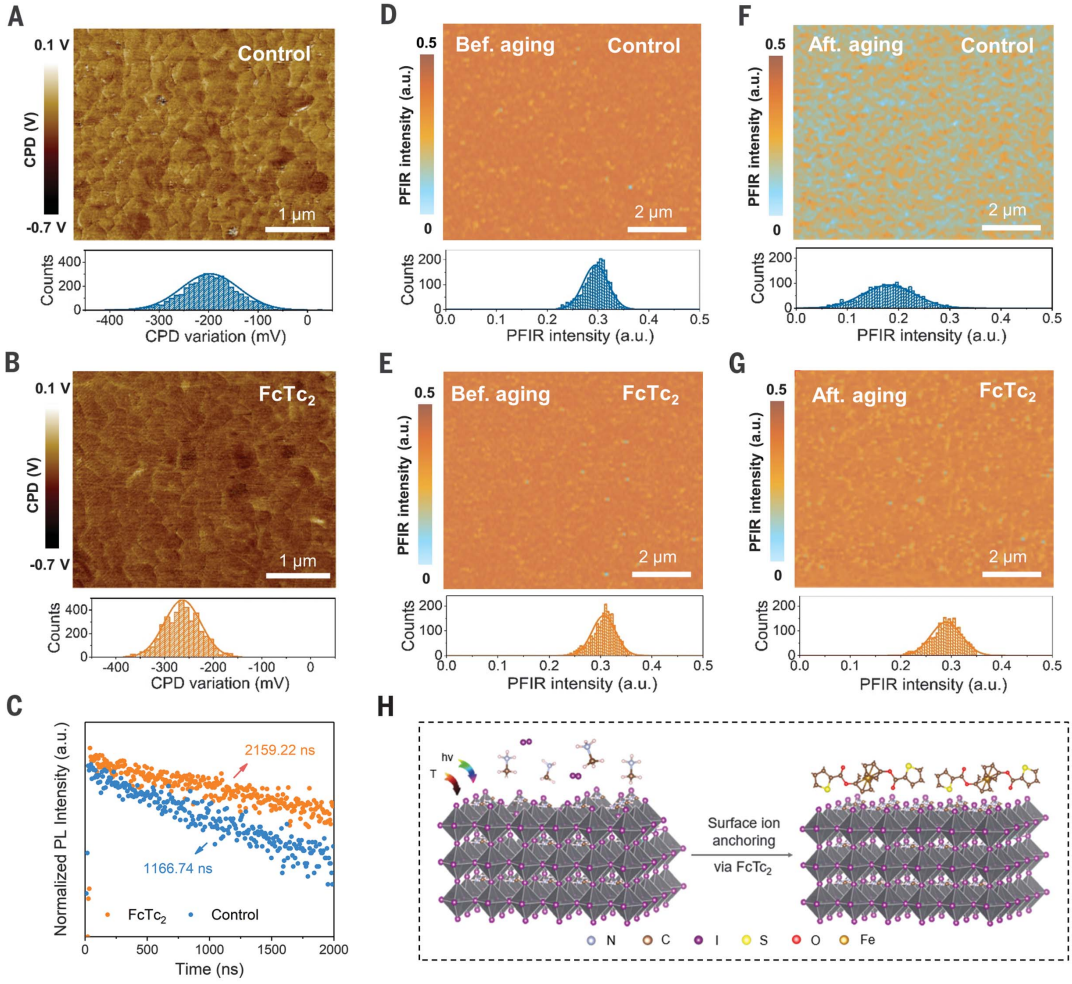

Fig. 2. Characterization of film surface properties. (**A** and **B**) Surface potential images were obtained by scanning KPFM of the control and $FcTc_2$-treated perovskite films. The statistical potential distributions of film surfaces are shown at the bottom. CPD, contact potential difference. (**C**) TRPL characterization of control and $FcTc_2$-treated perovskite films. PL, photoluminescence. (**D** to **G**) PFIR microscopy at an infrared (IR) frequency of 1480 cm^{-1} (which is resonant with the C-N stretching absorption of MA^+ ions) of control [(D) and (F)] and $FcTc_2$-modified perovskite films [(E) and (G)] before (Bef.) and after (Aft.) illumination at 85°C for 1000 hours. (**H**) Schematic illustration of the stabilization of surface ions by $FcTc_2$. T, temperature; hv, photon energy.

devices were also measured at the maximum power point (MPP) to obtain a stabilized photocurrent of 23.68 mA cm^{-2} and a stabilized PCE of 24.2% (Fig. 3C). One of the best-performing devices was validated by an independent solar cell–accredited laboratory (National Institute of Metrology, China) for certification, where a PCE of 24.3% (with V_{OC} = 1.179 V, J_{SC} = 25.59 mA cm^{-2}, and FF = 80.60%) was confirmed (fig. S20), which is the highest certified efficiency among all inverted PSCs to date (table S3). The PCEs also exhibited a satisfying reproducibility, with an average PCE of 22.5% for the control device and 24.5% for the $FcTc_2$-based device (Fig. 3D). The particular effectiveness of $FcTc_2$ is further verified in figs. S21 to S24 and table S4.

Additionally, we conducted quantitative analysis of the photovoltage loss (V_{OC} loss) for the control and $FcTc_2$-treated devices according to detailed balance theory (*26*). The EQE_{EL} values of 1.5 and 7.0% for the control device and the device with $FcTc_2$, respectively, could be obtained from electroluminescence (EL) spectra (Fig. 3, E and F), leading to 108.57 and 68.75 mV of ΔV_3 (V_{OC} loss from the nonradiative recombination), respectively. The relative lower ΔV_3 suggests that $FcTc_2$ suppresses nonradiative recombination as an interfacial modifier. The values of the three components of V_{OC} loss (ΔV_1, ΔV_2, and ΔV_3) are calculated in the supplementary text and summarized in table S5. A V_{OC} loss of 363 mV is one of the lowest values reported among inverted PSCs (*16*, *26*).

To investigate the effect of $FcTc_2$ functionalization on device stability, the efficiency evolution under various conditions was monitored. We first examined the long-term operational stability of unencapsulated devices by loading at MPP voltage under continuous 1-sun illumination in an N_2 atmosphere (Fig. 4A). The $FcTc_2$-functionalized device retained its initial PCE in the first 200 hours and only exhibited a decay of <2% after >1500 hours. In comparison, the control device decreased to 72% of its initial PCE. We further measured the stability of unencapsulated devices under heat and ambient conditions. As shown in figs. S27 and S28, the performance of the control devices dropped to <80% of the initial efficiency after >800 hours. By contrast, the $FcTc_2$-functionalized devices showed a T98 (time to 98% of initial PCE) of 2000 hours under an ambient environment and 1500 hours under continuous heating. Because the chemically reactive components (such as MA^+ and I^-) at the perovskite surface can readily volatilize and migrate through photo-, humidity, and thermal degradation (*27*, *28*), we inferred that

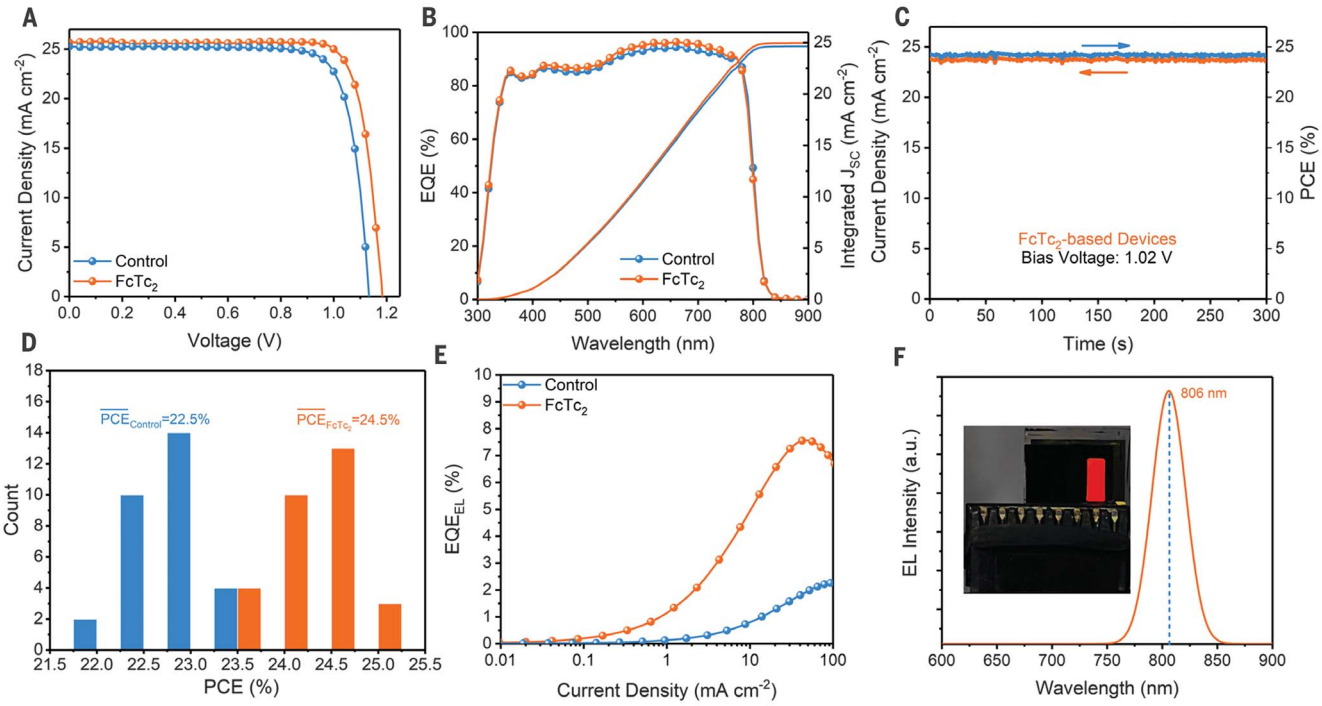

Fig. 3. Photovoltaic performance of PSCs. (**A**) *J-V* curves of the best-performing devices with and without $FcTc_2$. (**B**) EQE spectra and integrated current densities of the best-performing devices with and without $FcTc_2$. (**C**) Stabilized power output at the MPP for the best-performing PSCs treated with $FcTc_2$. (**D**) Histogram of the PCE values among 30 devices with and without $FcTc_2$. (**E**) EQE_{EL} values of the PSCs with and without $FcTc_2$ operating in light-emitting diode (LED) mode under different voltages. (**F**) EL spectra of the $FcTc_2$-based PSC operating as an LED.

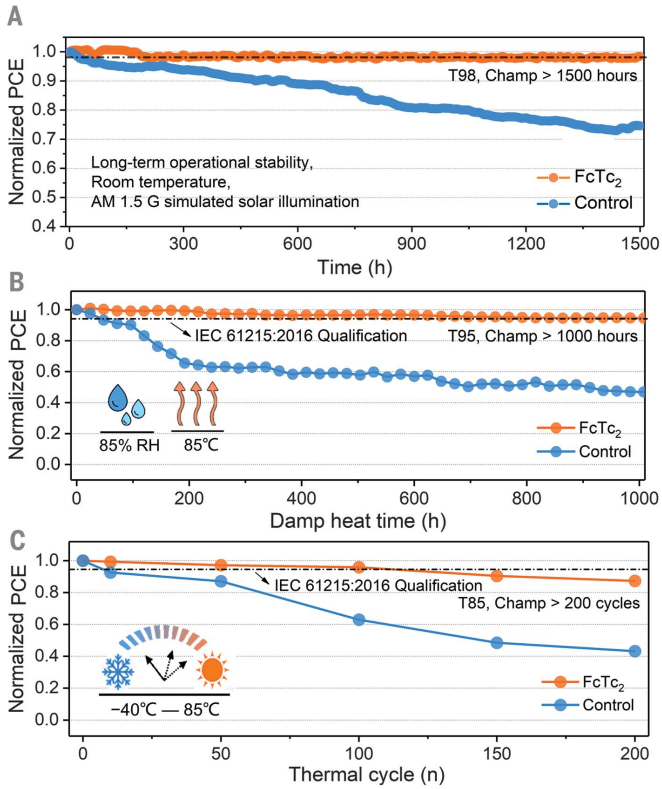

Fig. 4. Stability measurements of PSCs. (**A**) Normalized PCE of the unencapsulated PSCs with or without $FcTc_2$ measured at MPP under continuous 1-sun illumination in an N_2 atmosphere and at room temperature. (**B** and **C**) Normalized PCE of the PSCs with or without $FcTc_2$ measured following the IEC61215:2016 standards. (B) Encapsulated devices stored in 85% RH and 85°C in the dark. (C) Encapsulated devices stored in −40°C (15-min dwell) to 85°C (15-min dwell), ramp rate of 100°C $hour^{-1}$.

$FcTc_2$ enhances stability through the formation of additional bonding with perovskite surface ions and prevents any easily mobile ions from migration.

Additionally, we conducted strict stability measurements following the IEC61215:2016 standard, which is the most-used international standard for mature photovoltaic technologies. As shown in Fig. 4B, the $FcTc_2$-modified devices exhibited a T95 of >1000 hours under the damp heat test (85°C and 85% RH) and thus successfully passed the main point of IEC61215:2016 qualification for damp and heat conditions. Moreover, under the cycle shocks of cold (−40°C) and heat (85°C) shown in Fig. 4C, >85% PCE was retained after 200 cycles for the $FcTc_2$-modified devices, outperforming the control devices (40% PCE retained after 200 cycles). Taken together, these data indicate that $FcTc_2$-functionalized PSC devices exhibit excellent efficiency and stability and have the potential to move toward commercialization and rival traditional silicon solar cells.

REFERENCES AND NOTES

1. National Renewable Energy Laboratory, "Best research-cell efficiency chart" (2022); www.nrel.gov/pv/cell-efficiency.html.
2. L. Meng, J. You, Y. Yang, *Nat. Commun.* **9**, 5265 (2018).
3. G. Yang *et al.*, *Nat. Photonics* **15**, 681–689 (2021).
4. Y. Rong *et al.*, *Science* **361**, eaat8235 (2018).
5. J.-P. Correa-Baena *et al.*, *Science* **358**, 739–744 (2017).
6. N. Li, X. Niu, Q. Chen, H. Zhou, *Chem. Soc. Rev.* **49**, 8235–8286 (2020).

7. S. Yang *et al*., *Science* **365**, 473–478 (2019).
8. X. Zheng *et al*., *Nat. Energy* **5**, 131–140 (2020).
9. S. Wu *et al*., *Nat. Nanotechnol.* **15**, 934–940 (2020).
10. S. Wu *et al*., *Joule* **4**, 1248–1262 (2020).
11. S. Chen *et al*., *Science* **373**, 902–907 (2021).
12. S. Bai *et al*., *Nature* **571**, 245–250 (2019).
13. A. Mei *et al*., *Joule* **4**, 2646–2660 (2020).
14. D. Luo *et al*., *Science* **360**, 1442–1446 (2018).
15. J. J. Yoo *et al*., *Nature* **590**, 587–593 (2021).
16. F. Li *et al*., *J. Am. Chem. Soc.* **142**, 20134–20142 (2020).
17. Y. Guo *et al*., *Nat. Commun.* **12**, 644 (2021).
18. R. Wang *et al*., *Science* **366**, 1509–1513 (2019).
19. M. I. Saidaminov *et al*., *Nat. Mater.* **19**, 412–418 (2020).
20. N. Li *et al*., *Science* **373**, 561–567 (2021).
21. J. T. DuBose, P. V. Kamat, *J. Phys. Chem. Lett.* **10**, 6074–6080 (2019).
22. J. Zhang *et al*., *Nanoscale* **10**, 5617–5625 (2018).
23. A. N. Singh *et al*., *Adv. Energy Mater.* **10**, 2000768 (2020).
24. L. K. Ono, S. F. Liu, Y. Qi, *Angew. Chem. Int. Ed.* **59**, 6676–6698 (2020).
25. D. S. Jakob *et al*., *Angew. Chem. Int. Ed.* **59**, 16083–16090 (2020).
26. J. Wang *et al*., *Nat. Commun.* **11**, 177 (2020).
27. Q. Wang *et al*., *Energy Environ. Sci.* **10**, 516–522 (2017).
28. Z. Fan *et al*., *Joule* **1**, 548–562 (2017).

ACKNOWLEDGMENTS

Z.Z. thanks A. K.-Y. Jen and C. S. Lee for help and support. **Funding:** This work was supported by the New Faculty Start-up Grant of the City University of Hong Kong (9610421); the Innovation and Technology Fund (ITS/095/20); the ECS grant (21301319) and a GRF grant (11306521) from the Research Grants Council of Hong Kong; the Natural Science Foundation of Guangdong Province (2019A1515010761); and the Imperial College London Frankland Chair Endowment. N.J.L. is grateful for a Royal Society Wolfson Research Merit award. **Author contributions:** Z.L., B.L., and X.W. contributed equally to this work. Z.Z. conceived the ideas and designed the project with N.J.L. Z.Z. and N.J.L. directed and supervised the research. Z.L. fabricated the devices, conducted the characterization, and analyzed the data. B.L. and X.W. also contributed to the characterization and data analyses. N.J.L. and S.A.S. designed and synthesized the materials. S.Z. conducted the DFT calculations. D.G. conducted the stability tests. Z.L., B.L., X.W., N.J.L., and Z.Z. drafted and finalized the manuscript. All the authors revised the manuscript. **Competing interests:** A patent application based on this work has been submitted by Imperial College London and City University of Hong Kong, led by N.J.L. and Z.Z. The authors declare no other competing interests. **Data and materials availability:** All data needed to evaluate the conclusions in the paper are present in the paper or the supplementary materials.

SUPPLEMENTARY MATERIALS

science.org/doi/10.1126/science.abm8566
Materials and Methods
Supplementary Text
Figs. S1 to S28
Tables S1 to S5
References (*29*–*44*)

21 October 2021; accepted 17 March 2022
10.1126/science.abm8566

Science

Organometallic-functionalized interfaces for highly efficient inverted perovskite solar cells

Zhen LiBo LiXin WuStephanie A. SheppardShoufeng ZhangDanpeng GaoNicholas J. LongZonglong Zhu

Science, 376 (6591), • DOI: 10.1126/science.abm8566

Organometallics stabilizing perovskites

Perovskite solar cells with inverted (p-i-n) structure can have greater stability and lifetimes than conventional n-i-p structures but usually have somewhat lower power conversion efficiencies (PCEs). Li *et al*. report that an organometallic compound, ferrocenyl-bis-thiophene-2-carboxylate, can stabilize a multication perovskite layer of an inverted perovskite solar cells. After 1500 hours of maximum power point operation, 98% of the 25.0% PCE was maintained. The solar cell also exhibited high stability in damp heat tests. —PDS